Observation of the Fe spin spiral structure in Fe/Sm-Co exchange-spring bilayers by Mossbauer spectroscopy

doi: 10.1103/PhysRevB.68.064416

Observation of the Fe spin spiral structure in Fe/Sm-Co exchange-spring bilayers by Mössbauer spectroscopy

V. E. Kuncser,* M. Doi,† W. Keune,‡ M. Askin,§ and H. Spies
Institut für Physik, Universität Duisburg-Essen, D-47048 Duisburg, Germany

J. S. Jiang, A. Inomata,‖ and S. D. Bader
Materials Science Division, Argonne National Laboratory, Argonne, Illinois 60439, USA
(Received 25 February 2003; published 21 August 2003)

The in-plane Fe spin spiral structure for Fe/Sm-Co($1\bar{1}00$) exchange-spring magnetic bilayers was investigated by ^{57}Fe conversion electron Mössbauer spectroscopy during the magnetization reversal process, and correlated with hysteresis loops measured via the longitudinal magneto-optic Kerr effect. A direct experimental proof for a relaxed spiral angular spin distribution in the Fe layer is presented. Under negative applied fields the interfacial Fe spins rotate by up to 40° with respect to the easy axis of the Sm-Co hard-magnet layer.

DOI: 10.1103/PhysRevB.68.064416 PACS number(s): 76.80.+y, 75.70.−i, 75.60.Jk, 75.25.+z

I. INTRODUCTION

Exchange spring behavior is due to the interfacial exchange coupling of a soft magnetic phase to a hard magnetic phase. The hard magnetic phase provides the system with high anisotropy and coercivity, whereas the soft magnetic phase increases the saturation magnetization, resulting in an enhanced energy product of the composite two-phase system. Due to their unusually high remanence, large energy product, and low cost,[1–4] such exchange spring nanocomposite systems have applications as permanent magnets. Micromagnetic calculations and experimental results have shown that the intrinsic coercivity and the magnetic remanence are linearly reduced by increasing the amount of the soft phase,[2,5] whereas the exchange couplings depend strongly on the grain size of the two phases. Therefore, nanocomposite exchange spring magnets have the advantage of controlling magnetic performances via the preparation conditions. The challenge is to evolve suitable microscopic models for their quantitative description, since these materials are complex systems. In this respect, soft/hard magnetic bilayers could provide simple and convenient systems for both theoretical and experimental studies of the microscopic spin structure related to exchange spring behavior.

The magnetization reversal process in a soft magnetic film, ferromagnetically coupled to a hard magnetic layer with uniaxial in-plane anisotropy, was initially studied by Goto *et al.*[6] under the assumption that the hard layer is perfectly rigid and the soft layer has no anisotropy. For thick enough soft layers ($t \geqslant 50$ nm), the spins in the soft layer remain parallel to the easy axis of the hard layer for negative in-plane applied fields, H_{app}, less than an exchange field, H_{ex}, which is dependent on geometric and magnetic parameters of the soft layer (the exchange interaction, the thickness, and the saturation magnetization). At higher applied fields, the spins in the soft layer exhibit continuous in-plane rotations, as in a Bloch wall, with the rotation angle increasing with distance from the hard layer. For a much thinner soft layer (approaching the domain-wall width in the hard layer), the soft layer is expected to be rigidly magnetically coupled to the hard layer, switching together with it at a nucleation field that depends on the geometric and magnetic characteristics of both the soft and hard layers. In real systems, the soft layer may have a finite anisotropy and an intermediate thickness between the two cases described above. In such cases the hysteresis loops show both an exchange field, H_{ex}, where the spins in the soft layer start to rotate towards the negative applied field direction, and an irreversible field, H_{irr}, where the hard layer switches irreversibly.[7] Further theoretical models for describing exchange-spring layered systems have analyzed the spin structure of the hard/soft system as a one-dimensional chain of representative spins. Each representative spin belongs to an elementary layer, parallel to the interface, with a finite size and given depth. The chain is normal to the interface and the representative spins are assumed to show different rotations under the influence of the negative field, depending on the layer depth. The final angular spin configuration is obtained by an iterative process based on the energy minimization procedure under the assumption that even deeper spins in the hard layer are allowed to rotate in the film plane.[7–10] According to this model, between the exchange field and the irreversible field, a spiral spin structure which extends across the whole soft-layer thickness and partially also into the hard layer is formed. Such a spin structure was observed in $Ni_{80}Fe_{20}/Fe_{55}Pt_{45}$ exchange spring bilayers via polarized neutron reflectivity measurements.[11]

The present paper describes the microscopic observation of the spin structure in the soft magnetic layer of the Fe/Sm-Co($1\bar{1}00$) exchange spring magnetic bilayer system during the magnetization reversal process. The spin structure, obtained by ^{57}Fe conversion electron Mössbauer spectroscopy (CEMS), is correlated with longitudinal magneto-optic Kerr effect (MOKE) data and is discussed in terms of theoretical models.

II. EXPERIMENTAL AND METHODOLOGICAL DETAILS

The interfacial spin structures of magnetic atoms as well as their local structure and symmetry can be analyzed with a

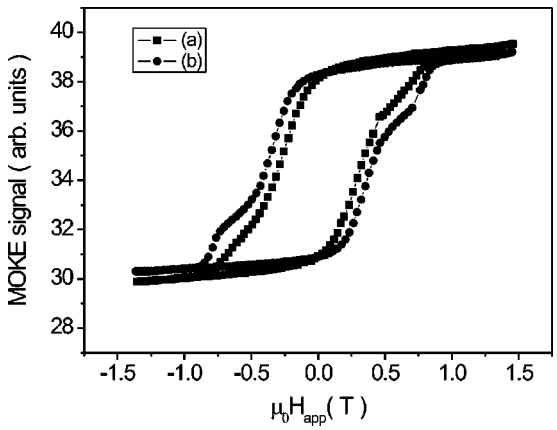

FIG. 1. Longitudinal MOKE hysteresis loops for sample A (homogeneous ^{57}Fe film) (a), and sample B (^{57}Fe at interface) (b).

high depth selectivity by using ^{57}Fe CEMS, combined with the ^{57}Fe tracer layer technique, i.e., with isotopically enriched ^{57}Fe probe layers (resolution limit of less than 1nm) at the interface or at different depths.[12–14] The only limitation for a suitable study of the spin structure is that the analyzed system should contain atoms with reasonably large magnetic moments, giving rise to high enough magnetic hyperfine fields, H_{hf}, in order to measure the line intensity ratios in the Zeeman-split Mössbauer sextet.[15]

The soft/hard bilayer systems were prepared via dc magnetron sputtering onto MgO(110) single crystals, with Cr as buffer and cap layers[7,16] and in the sequence: MgO(110)/Cr(20 nm)/Sm-Co(10 nm)/Fe(15 nm)/Cr(5 nm). The epitaxial relationship for the magnetically hard Sm-Co($1\bar{1}00$) layer with nominal composition Sm_2Co_7 is Sm-Co[0001]//Cr[$01\bar{1}$]//MgO[001]. Accordingly, a uniaxial in-plane spin structure is expected for the hard magnetic phase, with the magnetic easy axis parallel to the hexagonal Sm-Co *c* axis. Two types of samples with different ^{57}Fe layers (enriched to 95% in ^{57}Fe) were prepared. In the first type (sample A) the entire soft magnetic layer (15 nm) is homogeneously enriched in ^{57}Fe, whereas in the second type (sample B) only a 2-nm-thick ^{57}Fe tracer layer was deposited at the interface with the hard phase, the remainder of the soft phase being natural Fe (only $\sim$2% ^{57}Fe isotopic abundance). Therefore, the Mössbauer signal of sample B originates predominantly from the interfacial probe layer.

Longitudinal MOKE measurements were taken using *p*-polarized, 633-nm He-Ne laser light, and with the applied field parallel to the Sm-Co easy axis. Samples A and B have similar hysteresis loop, as shown in Fig. 1. As the result of the finite penetration of the light, the MOKE measurements are dominated by the switching of the Fe layer. The sharp drop in the MOKE signal at $H_{ex} \sim -0.15(5)$ T indicates the onset of Fe layer magnetization rotation. The MOKE signal continues to decrease with increasing applied reversal field, as more and more moments in the Fe layer rotate toward the field. At $H_{irr} \sim -0.65(5)$ T, the Sm-Co layer switches irreversibly.

The spin configuration in the ^{57}Fe layer during the magnetization reversal process was investigated at room temperature by ^{57}Fe CEMS using a home-made He-CH_4 proportional counter in applied fields, H_{app}, up to 0.9 T for sample A. A field of only 0.6 T could be applied for sample B due to the fairly weak Mössbauer signal and the substantial lowering of the count rate in high fields. A Mössbauer drive system operating in constant acceleration mode combined with conventional electronics and a ^{57}Co(Rh matrix) source of $\sim$50 mCi activity were employed.

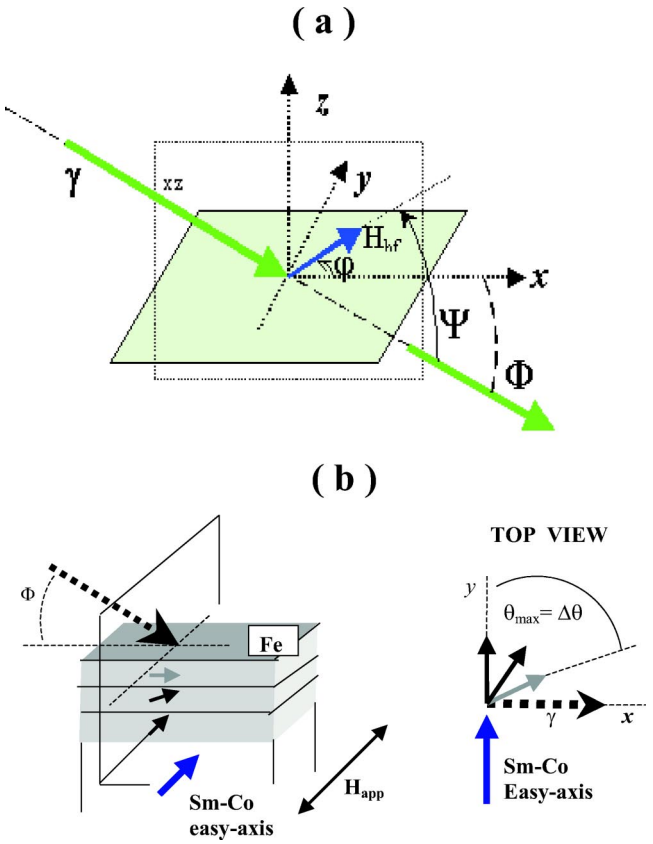

FIG. 2. (a) Schematic geometrical arrangement of the CEMS measurement. ϕ is 20° for sample A and 30° for sample B. The magnetic field is applied along the Sm-Co easy axis (the *y* axis). (b) Schematic representation of a rigid spin spiral distribution in the plane of the soft magnetic layer, with interfacial Fe spins aligned parallel to the Sm-Co easy axis during the magnetization reversal process in applied negative fields lower than H_{irr}. The γ radiation is perpendicular to the applied field direction.

It is well known that the Fe spin configuration can be analyzed starting from the intensity ratio between the second (or fifth) and the third (or fourth) line, $R_{23} = I_2/I_3$, of the Zeeman-split Mössbauer sextet.[15] If the hyperfine field (which is anti-parallel to the spin direction) of an Fe atom forms an angle ψ with the Mössbauer γ-ray direction, then $R_{23} = 4\sin^2\psi/(1+\cos^2\psi)$. For in-plane distributed spins analyzed with incident γ radiation perpendicular to the sample plane ($\psi = 90°$), the above intensity ratio is insensitive to the in-plane spin direction ($R_{23} = 4$). Therefore, the spin configuration in layered samples with in-plane Fe spins may be analyzed only in a non-perpendicular geometry, with the radiation incident at an angle ϕ vs the sample plane [Fig. 2(a)]. If the spin directions follow a certain angular distribution,

$P(\varphi)$, in the sample plane (where φ is the azimuth angle relative to the x axis), the intensity ratio may be expressed by the relationship[17]

$$R_{23}=4\int_0^{2\pi}\frac{1-\cos^2\phi\cos^2\varphi}{1+\cos^2\phi\cos^2\varphi}P(\varphi)d\varphi$$

$$\text{with}\quad \int_0^{2\pi}P(\varphi)d\varphi=1. \tag{1}$$

The above intensity ratio can be theoretically evaluated for different model spin distributions, $P(\varphi)$, as a function of the distribution parameters and the relative orientation, ϕ, between the sample and the radiation. The distribution parameters are evaluated by equating the theoretical expression given by Eq. (1) to the experimental intensity ratio R_{23}, for a number of experimental spectra which must be at least equal to the number of the distribution parameters.[17]

The two samples were initially magnetized to saturation in an applied field of 1.5 T parallel to the direction of the Sm-Co easy axis. Subsequently, the CEMS measurements were performed with the γ radiation perpendicular to the applied magnetic field [Sm-Co easy axis//H_{app}//y axis, Fig. 2(b)] and incident under an angle ϕ of $20°\pm5°$ onto sample A. In order to increase the count rate, the incidence angle ϕ of the γ radiation on sample B was increased to $30°\pm5°$. The spectra were sequentially acquired starting with the highest positive field value (the applied field pointing in the same sense as the saturation field) and then decreasing the field stepwise to zero. Subsequently, the field was again sequentially increased, but in the opposite sense (negative applied field direction). In order to find the out-of-plane spin component in the Fe soft magnetic layer, additional measurements on both samples were performed in perpendicular geometry ($\phi=90°$).

III. RESULTS AND DISCUSSION

A. Perpendicular γ-ray incidence

The Mössbauer spectra of the two samples taken in perpendicular geometry ($\phi=90°$) and in zero applied field are presented in Fig. 3. The Mössbauer pattern of sample A was fitted with a Lorentzian sextet, showing a narrow linewidth (full width at half maximum) of 0.34(1) mm/s, negligible isomer shift and quadrupole splitting, and a hyperfine magnetic field of 33.2(1) T typical for bcc-Fe. For sample B, the broader and asymmetrical six-line magnetic pattern could be suitably fitted only by using two Lorentzian sextets, with linewidths of 0.34(1) mm/s, negligible isomer shifts and quadrupole splittings, and hyperfine magnetic fields of 33.1(1) T and 35.3(1) T, respectively. By correlating the measured relative spectral areas of the two sextets of sample B (66% and 33%, respectively) with the respective hyperfine field values, we conclude that the outer sextet (enhanced hyperfine field of 35.3 T) belongs to a 0.7-nm-thick interfacial Fe-rich bcc alloy containing Co impurities from the Sm-Co underlayer, whereas the inner sextet (with a lower hyperfine field of 33.1 T) is assigned to the bulklike bcc-Fe sites in the residual 1.3-nm-thick ^{57}Fe probe layer. The R_{23} values of samples A and B obtained in perpendicular geometry ($\phi=90°$) in different applied fields were always equal to 4.0(1), demonstrating in-plane orientation of the Fe spins during the magnetization reversal process.

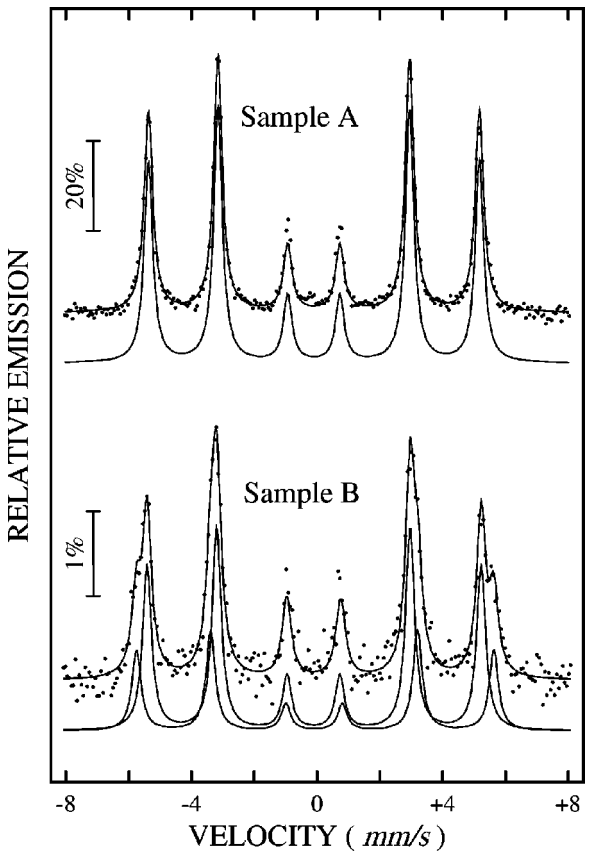

FIG. 3. Room temperature CEM spectra of samples A and B, taken in a perpendicular geometry ($\phi=90°$) and a zero applied field.

B. Inclined γ-ray incidence: homogeneous ^{57}Fe film

Typical Mössbauer spectra of sample A, taken under an angle of incidence of $\phi=20°$ and in different applied fields, are presented in Fig. 4(a). It is observed that the spectra exhibit a remarkable variation of the R_{23} intensity ratio vs H_{app}. The applied field dependence of the experimental R_{23} ratio of sample A is plotted in Fig. 5(a). Accordingly, the intensity ratio decreases from nearly 4 at the highest positive field, $H_{app}=0.90$ T, down to a minimum value of 1.50(11) at a critical negative field of $-0.33(5)$ T, and then increases again at higher negative fields.

In agreement with a spiral Fe spin structure, where the in-plane rotation angle φ of the spins in the Fe layer increases linearly with the distance from the hard layer, we assume that, in the overall soft magnetic layer, the in-plane angular spin distribution (if projected onto the film plane) is of step-shape type (or fanlike), i.e., the Fe spins are uniformly distributed inside a field dependent aperture, $\Delta\varphi$ [Fig. 2(b)]. The mathematical expression of this angular distribution is $P(\varphi)=P_0$ for $\varphi_0<\varphi<\varphi_0+\Delta\varphi$ and $P(\varphi)=0$ in the

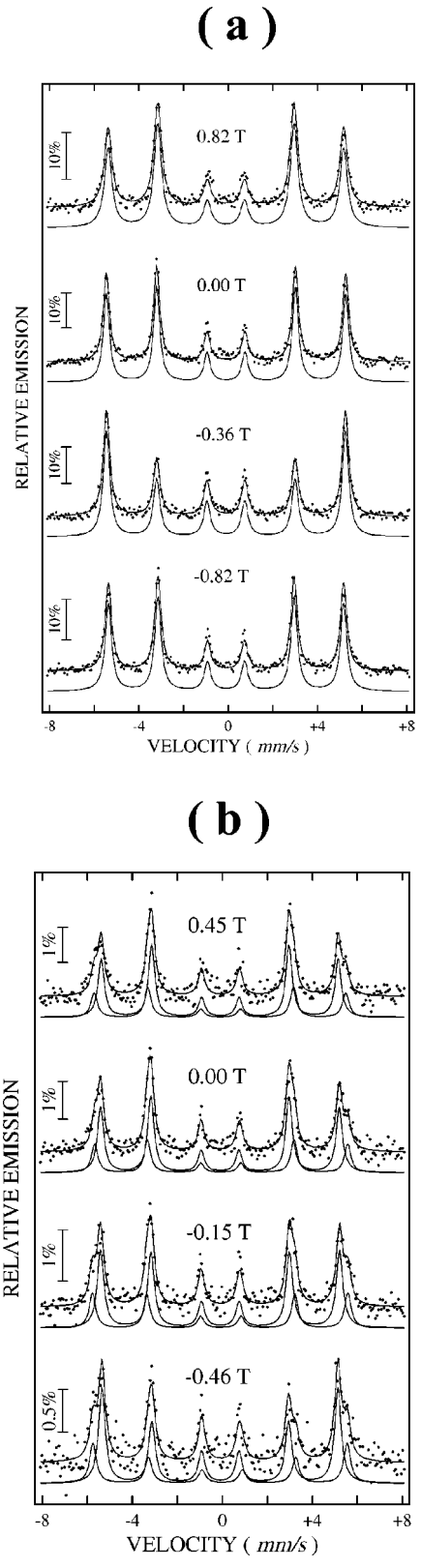

FIG. 4. (a) Room temperature CEM spectra of sample A, taken with the γ radiation under an angle of incidence ϕ of 20° and in different applied fields. (b) Room temperature CEM spectra of sample B, taken with the γ radiation under an angle of incidence ϕ of 30° and in different applied fields.

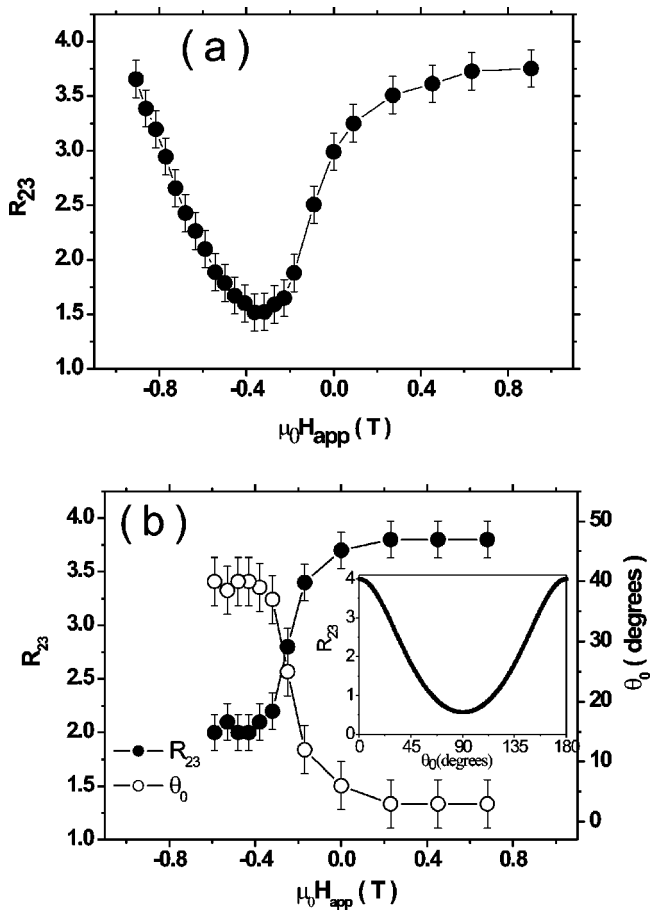

FIG. 5. (a) Experimental intensity ratio R_{23} vs the applied field, obtained from least-square fitting the CEM spectra of sample A. (b) Experimental intensity ratio R_{23} and interfacial Fe spin orientation, θ_0, vs the applied field, obtained from least-square fitting the CEM spectra of sample B. The theoretical intensity ratio calculated from Eq. (3) for a unidirectional angular spin distribution is shown in the inset.

rest of the 2π interval, with $\Delta\varphi$ dependent on H_{app}. Theoretically, the R_{23} intensity ratio can be obtained in this approximation by employing Eq. (1).

Two peculiarities have to be mentioned for our systems: (i) for our chosen geometry [Fig. 2(b)], the γ radiation is incident onto the sample plane perpendicular to the direction of the applied magnetic field and, hence, to the Sm-Co easy axis (y axis), and (ii) the ^{57}Fe conversion electrons carrying the information about the Fe spin direction at different depths will escape at the sample surface with different probabilities (or weights) from different depths and contribute to the overall Mössbauer pattern accordingly. Connected with item (i) it is more convenient to describe the in-plane Fe spin direction at different depths of the soft layer by taking the direction of the Sm-Co easy axis, i.e., the y axis in Fig. 2(a), as a reference. Therefore, we express Eq. (1) further by the new in-plane angle θ with respect to the y axis, defined by $\theta=\pi/2-\varphi$. Concerning item (ii), the spin angular probability at different depths should be modulated with the transmission weight function of the conversion electrons, $T_t(z)$, which gives the relative number of electrons starting from a

given depth z and escaping at the material surface with all possible energies and in all directions.[18] The transmission weight functions may be obtained by the integration over all the escaping energies of the partial weight functions, $T(z,E)$, giving the probability that electrons generated at a depth z in the material escape at the surface in all the possible directions with a certain energy, E. Here, the ^{57}Fe K-conversion electrons of 7.3 keV in energy are relevant. From Monte Carlo simulations, Liljequist *et al.*[18] obtained the K conversion electron transmission weight functions corresponding to different depths.[19] An almost linear decrease of $T_t(z)$ vs z was obtained for depths lower than 30 nm, with a slope approaching $-2.7/r_B$, with r_B the Bethe range of K electrons. Taking into account that $r_B \approx 320$ nm in metallic Fe, a value of about 0.008 nm^{-1} may be deduced for this slope, and $T_t(z) \approx 1 - 0.008\, z$. Because the density of Cr and Fe are close, we assume that the same expression for $T_t(z)$, in both the 15-nm soft magnetic layer as well as the Cr cap layer, is valid. Consequently, $T_t(z)$ for the present system (sample A) will increase linearly with depth z from a value of about 0.6 at 20 nm (the depth of the Fe/Sm-Co interface) up to a value of about 0.74 at 5 nm (the depth of the upper part of the Fe layer). In agreement with the spiral spin distribution model for the Fe spins in the soft magnetic layer, it is assumed that in a negative applied field the Fe spins at the Fe/Sm-Co interface are oriented at an in-plane angle θ_0 relative to the Sm-Co easy axis (y axis), and that the angular deviation increases linearly with the distance from the interface up to an in-plane angle $\theta_0 + \Delta\theta$, at the upper boundary of the Fe layer. Based on items (i) and (ii) above, Eq. (1) may be expressed as:

$$R_{23} = \frac{4}{0.67 \cdot \Delta\theta} \int_{\theta_0}^{\theta_0 + \Delta\theta} \frac{1 - \cos^2\phi \sin^2\theta}{1 + \cos^2\phi \sin^2\theta} \times \left(0.60 + \frac{0.14 \cdot (\theta - \theta_0)}{\Delta\theta} \right) d\theta. \quad (2)$$

From Eq. (2) R_{23} can be calculated for different apertures of the spiral, $\Delta\theta$, and starting angles, θ_0. Typical results obtained by the numerical integration of Eq. (2) are presented in Fig. 6. It is worth mentioning that for the thickness of our samples, the depth dependence of the weight function, $T_t(z)$, induces only minor variations of the R_{23} intensity ratio (less than 0.11), generally lower than the statistical or the experimental errors.

In the first step, the analysis of the spin structure in the Fe layer of sample A was carried out under the assumption that during the magnetization reversal process, the interfacial Fe spins remain aligned along the direction of the Sm-Co easy axis ($\theta_0 = 0°$) up to the critical switching field (rigid spin spiral model). The geometry of the spin structure is sketched in Fig. 2(b). In order to find the spiral aperture $\Delta\theta$, corresponding to different applied fields, the experimental intensity ratios R_{23} presented in Fig. 5(a) should fit the upper curve (full squares) in Fig. 6, corresponding to $\theta_0 = 0°$. One can see that the spin aperture $\Delta\theta$ would continuously increase up to 180°, which (within the rigid spin spiral model) leads to a theoretical R_{23} value of 1.8. According to Fig. 5(a), this value is reached at an applied field of about -0.60 T. Physically, at higher negative fields, the spins should begin to respond more along the negative field direction, resulting in a decreasing aperture vs the applied field. Taking into account the symmetrical evolution of the intensity ratio presented in Fig. 6 [due to the 180° periodicity of the integral in Eq. (2)], a *decrease* of the intensity ratio is expected at some negative fields higher than 0.60 T. By contrast, the experimental ratio in Fig. 5(a) shows a continuous *increase* for negative fields higher than 0.60 T. Therefore, we conclude that the interfacial Fe spins are not rigidly pinned along the Sm-Co easy axis.

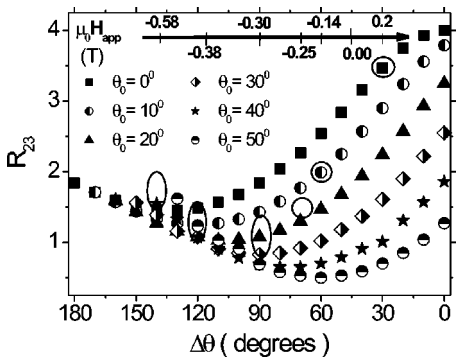

FIG. 6. Calculated intensity ratios R_{23} for sample A as a function of the angular Fe-spin distribution aperture $\Delta\theta$, obtained by numerical integration of Eq. (2) with θ_0 as a parameter. Some typical experimental data points and their corresponding applied fields values are indicated by large circles (for positive fields and negative fields <0.25 T) and by ellipses (for negative fields $\geqslant 0.30$ T) as examples. The experimental R_{23} values coincide with the theoretical dependencies within the shown circles or ellipses.

C. Inclined γ-ray incidence: interfacial ^{57}Fe layer

In order to obtain direct experimental information on the orientation of the interfacial Fe spins (which is expressed by the angle θ_0) we proceeded to study the magnetization reversal process in sample B by CEMS. Typical Mössbauer spectra taken in different in-plane applied fields and with the radiation incident at $\phi = 30°$, are presented in Fig. 4(b). The spectra were fitted with two sextets with Lorentzian line shapes (as mentioned above for perpendicular geometry) with similar intensity ratios R_{23} for both sextets. The evolution of the intensity ratio R_{23} vs the applied field is shown in Fig. 5(b). Since the Mössbauer signal originates mainly from the very thin 2-nm ^{57}Fe layer at the interface, a unidirectional spin distribution with $P(\theta) = C_1 \delta(\theta - \theta_0)$ can be assumed for this layer. Moreover, the weight function $T_t(z)$ becomes constant and, therefore, the intensity ratio can be simply expressed as

$$R_{23} = 4 \times \frac{1 - \cos^2\phi \sin^2\theta_0}{1 + \cos^2\phi \sin^2\theta_0}. \quad (3)$$

This theoretical dependence of the intensity ratio vs angle θ_0 is shown in the inset of Fig. 5(b). In Fig. 5(b) we also present the orientation θ_0 of the interfacial Fe spins relative to the Sm-Co easy axis vs H_{app} during the magnetization reversal process, as obtained by equating the experimental intensity ratio R_{23} [shown in the same Fig. 5(b)] to the theoretical dependence expressed by Eq. (3). It is observed that at negative applied fields of about 0.15 T the interfacial Fe spins begin a sharp rotation, and a maximum value of 40° is reached at about -0.40 T. It is worth mentioning that over this field interval the intensity ratio R_{23} in sample A [Fig. 5(a)] shows only a small variation of 0.2–0.3 around the minimum value of 1.50(11). At negative fields higher than 0.40 T, but lower than the experimental limit of 0.60 T ($H_{irr} < -0.60$ T), the interfacial Fe spins make a constant angle of 40° with the Sm-Co easy axis [Fig. 5(b)].

Once the direction of the interfacial Fe spins, θ_0, is known [Fig. 5(b)], the spiral aperture $\Delta\theta$ in the overall soft magnetic layer (sample A) may be graphically estimated from the theoretical dependencies in Fig. 6 and the experimental R_{23} results shown in Fig. 5(a). In this respect, for a given field, the aperture $\Delta\theta$ is obtained from the experimental ratio R_{23} by using the theoretical curve in Fig. 6 which was calculated for the interfacial orientation θ_0, assigned to the same field as R_{23}. This procedure works properly for all positive fields as well for negative fields lower than 0.25 T (see large circles in Fig. 6 as examples). At a field around -0.30 T, a minimum intensity ratio R_{23}^{expt}(min) of ≈ 1.50 is observed experimentally for the overall soft magnetic layer [Fig. 5(a)], simultaneously with an interfacial spin orientation with an angle $\theta_0 \approx 30°$ [Fig. 5(b)]. Therefore, the spiral aperture $\Delta\theta$ has to correspond to the minimum R_{23}^{theor}(min) of the theoretical R_{23} curve evaluated for $\theta_0 = 30°$, and, according to Fig. 6, its value is $\Delta\theta \approx 90°$. However, the theoretical value R_{23}^{theor}(min) of this minimum is about 0.60 lower than the experimental minimum R_{23}^{expt}(min) of 1.50(15) [Fig. 5(a)]. Such a difference between the theoretical and experimental R_{23} values may be related to the fact that our approximation of a linear relationship between θ and z is not valid at negative fields higher than 0.25 T. We assume that this difference of about $+0.6$ is a systematic deviation between experiment and our calculation and applies also at negative fields larger than 0.3 T. Therefore, as an approximation for negative fields higher than 0.38 T, where the interfacial spins are oriented under $\theta_0 = 40°$ [Fig. 5(b)], the apertures $\Delta\theta$ were obtained from that ordinate of the calculated $R_{23}(40°;\Delta\theta)$ curve (asterisks in Fig. 6) which is equal to the theoretical minimum R_{23}^{theor}(min) plus the increment $R_{23} - R_{23}^{expt}$(min) of the experimental intensity ratio R_{23} from its own minimum R_{23}^{expt}(min). (The corrected experimental ordinate R_{23}^{corr} is obtained by subtracting a value of 0.6 from the experimental intensity ratio R_{23}). The vertical axes of the ellipses in Fig. 6 show the differences between the experimental intensity ratios and the theoretical estimations at some selected negative field values larger than 0.25 T.

The evolution of the assumed step-shape type distribution parameters θ_0 and $\Delta\theta$ (which describe the in-plane projection of the Fe spin spiral) vs the applied magnetic field is shown in Fig. 7. One can observe that during the reversal process both, the aperture of the distribution and the deviation of the interfacial Fe spins from the Sm-Co easy axis, are increasing for higher negative fields, with a maximum increment per field unit at about -0.30 T. This is the same applied field where the magnetization in the hysteresis loop (Fig. 1) exhibits a maximum variation vs. the field. A schematic illustration of the Fe spin spiral structure at an applied field of -0.58 T is shown in Fig. 8.

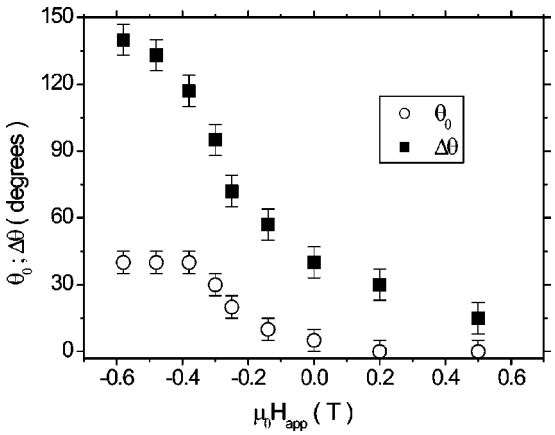

FIG. 7. Interfacial Fe spin orientation θ_0 and angular Fe-spin distribution aperture $\Delta\theta$ in the Fe layer vs the applied field.

IV. CONCLUSIONS

Two types of samples of Fe/Sm-Co($1\bar{1}00$) exchange-spring magnetic bilayers with different ^{57}Fe tracer layers were investigated by longitudinal MOKE and ^{57}Fe CEMS in applied magnetic fields. The in-plane spin structure in the Fe soft magnetic layer and at the Fe/Sm-Co interface during the magnetization reversal process was inferred from the evolution of the R_{23} intensity ratio in the Mössbauer sextets as a function of the applied field. The spin structure in the soft magnetic layer was determined under the assumption of a linear dependence between the spin orientation in an elemen-

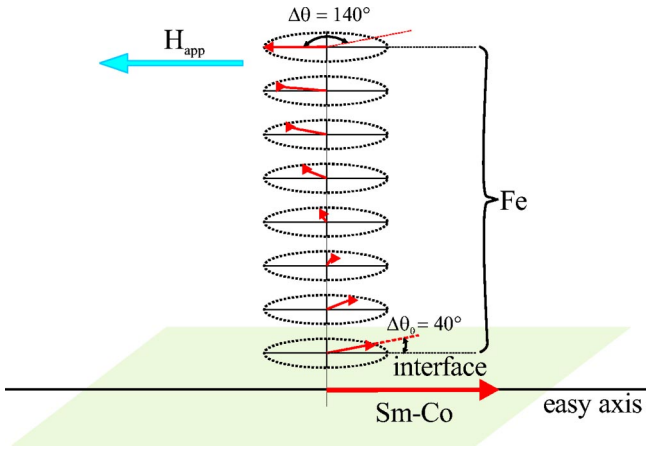

FIG. 8. Schematic illustration of the Fe spin spiral structure for a negative applied field of 0.58 T.

tary layer and the layer depth, in agreement with a uniform spin spiral model. Both the direction of interfacial Fe spins and the spiral aperture in the Fe layer were found to increase with the negative field. For negative fields lower than the irreversible switching field H_{irr}, the deviation of the interfacial Fe spin direction from the Sm-Co easy axis reaches a maximum of 40°, whereas the spin aperture in the Fe layer reaches 140°. These results agree qualitatively with earlier numerical calculations.[7] However, contrary to the theoretical models, it is experimentally proven that for negative applied fields lower than H_{irr}, the interfacial Fe spin rotation is blocked at a certain field, while the variation of the overall magnetization is related only to a change of the angular aperture of the Fe spin distribution. In order to measure the depth dependence of the angular Fe spin distribution in detail, thin ^{57}Fe probe layers need to be placed at different depths in the natural Fe layer.

Note added in proof. Recently, we learned that a direct observation of the Fe spin spiral structure in Fe/FePt exchange-spring bilayers by elastic forward nuclear resonance scattering of synchrotron radiation was achieved by R. Roehlsberger, H. Thomas, K. Schlage, E. Burkel, O. Leupold, and R. Rueffer.[20]

ACKNOWLEDGMENTS

The authors appreciate the valuable technical assistance by U.v. Hörsten (Duisburg). Work at Duisburg was supported by Deutsche Forschungsgemeinschaft (SFB 491). Work at Argonne was supported by the U.S. Department of Energy, Basic Energy Sciences-Materials Sciences, under Contract No. W-31-109-ENG-38. The financial support by Alexander-von-Humboldt Stiftung (V. Kuncser) and by Deutscher Akademischer Austauschdienst (M. Askin) is gratefully acknowledged.

*Permanent address: National Institute for Physics of Materials, P. O. Box MG7, RO-76900 Bucharest—Magurele, Romania.
†Permanent address: Department of Materials Science and Engineering, Nagoya University, Nagoya, Japan.
‡Electronic address: keune@uni-duisburg.de
§Permanent address: Faculty of Physics, Dicle University, Diyarbakir, Turkey.
‖Permanent address: Fujitsu Ltd., Atsugi, Japan.

[1] R. Coehoorn, D. B. de Mooji, J. P. W. B. Duchateau, and K. H. J. Buschow, J. Phys. (Paris), Colloq. **49**, C8-669 (1988).
[2] E. F. Kneller and R. Hawig, IEEE Trans. Magn. **27**, 3588 (1991).
[3] R. Skomski and J. M. D. Coey, Phys. Rev. B **48**, 15812 (1993).
[4] R. Fischer, T. Leineweber, and H. Kronmüller, Phys. Rev. B **57**, 10723 (1998).
[5] T. Schrefl and J. Fidler, IEEE Trans. Magn. **35**, 3223 (1999).
[6] E. Goto, N. Hayashi, T. Miyashita, and K. Nakagawa, J. Appl. Phys. **36**, 2951 (1965).
[7] E. E. Fullerton, J. S. Jiang, M. Grimsditch, C. H. Sowers, and S. D. Bader, Phys. Rev. B **58**, 12193 (1988).
[8] K. Mibu, T. Nagahama, and T. Shinjo, J. Magn. Magn. Mater. **163**, 75 (1998).
[9] T. Nagahama, K. Mibu, and T. Shinjo, J. Phys. D **31**, 43 (1998).
[10] K. Mibu, T. Nagahama, T. Shinjo, and T. Ono, Phys. Rev. B **58**, 6442 (1998).
[11] K. V. O'Donovan, J. A. Borchers, C. F. Majkrzak, O. Hellwig, and E. E. Fullerton, Phys. Rev. Lett. **88**, 067201 (2002).
[12] Ch. Sauer and W. Zinn, in *Magnetic Multilayers*, edited by L. H. Bennett and R. E. Watson (World Scientific, Singapore, 1993).
[13] M. Przybylski, Hyperfine Interact. **113**, 135 (1998).
[14] T. Shinjo and W. Keune, J. Magn. Magn. Mater. **200**, 598 (1999).
[15] G. K. Wertheim, *Mössbauer Effect: Principles and Applications* (Academic Press, New York, 1964).
[16] E. E. Fullerton, C. H. Sowers, J. P. Pearson, and S. D. Bader, Appl. Phys. Lett. **69**, 2438 (1996).
[17] V. Kuncser, W. Keune, M. Vopsaroiu, and P. R. Bissell, Nucl. Instrum. Methods Phys. Res. B **196**, 135 (2002).
[18] D. Liljequist, Scanning Electron Microscopy III, SEM Inc., AMF O'Hare (Chicago), IL 60666, USA (1983), pp. 997–1017, and references therein.
[19] D. Liljequist, T. Ekdahl, and U. Bäverstam, Nucl. Instrum. Methods **155**, 529 (1978).
[20] R. Roehlsberger, H. Thomas, K. Schlage, E. Burkel, O. Leupold, and R. Rueffer, Phys. Rev. Lett. **89**, 237201 (2002).